ACS OMEGA

Article

Cite This: ACS Omega 2018, 3, 7846−7855

Hierarchically Grown NiO-Decorated Polyaniline-Reduced Graphene Oxide Composite for Ultrafast Sunlight-Driven Photocatalysis

Preety Ahuja,[†,‡] Sanjeev Kumar Ujjain,[‡] Indu Arora,[§] and Mohammed Samim*[,†]

[†]Department of Chemistry, Jamia Hamdard, Hamdard Nagar, Delhi 110062, India

[‡]Center for Energy and Environmental Science, Shinshu University, 4-17-1 Wakasato, Nagano-City 380-8553, Japan

[§]Department of Biomedical Sciences, Shaheed Rajguru College of Applied Sciences for Women, Vasundhra Enclave, Delhi 110096, India

Supporting Information

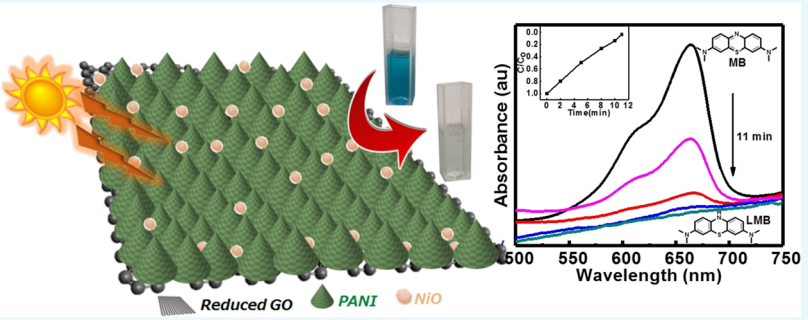

ABSTRACT: Polymers and transition-metal oxides have gained great interest as a photocatalyst in environmental remediation. They could be modified with each other in order to improve their activity. Here, a sunlight-responsive hierarchically structured ternary composite of nickel oxide, polyaniline, and reduced graphene oxide (NiO@PANI/RGO) has been synthesized and employed as a catalyst for dye [methylene blue (MB)] degradation. PANI/GO synthesized by interfacial polymerization acts as a matrix for the growth of NiO using a microemulsion solvothermal method, ensuing an in situ reduction of graphene oxide during the formation of a hierarchical NiO@PANI/RGO composite. Morphological studies of the as-synthesized NiO@PANI/RGO composite reveal fine NiO (10 nm) nanoparticles intercalated between the uniformly grown PANI spines (50−60 nm) over the RGO surface. The optical band gap of ∼1.9 eV calculated from the UV−vis spectrum illustrates the extended light absorption range for the NiO@PANI/RGO photocatalyst. The efficiency of 98% MB degradation within 11 min with the degradation rate constant 0.086 min^{-1} for NiO@PANI/RGO has surpassed any other report on metal oxide/graphene-based ternary composites. Overall, this work could pave the way for the fabrication of futuristic hierarchical structured ternary nanocomposites as an efficient photocatalyst and facilitate their application in the environmental protection issues.

1. INTRODUCTION

With industrialization and population growth, the environmental contamination caused by organic pollutants has become a pivotal issue all over the world. Also, effluents from various industries, particularly dyes, are the major source causing damage to living organisms.[1−4] They, being nonbiodegradable, can eventually decrease the dissolved oxygen capacity of water, thereby disturbing the natural ecological balance.[5] Therefore, the management of these nonaffable wastes is the need of hour toward a clean and healthy environment.

Earlier, an assortment of efforts has been conceded to surmount these environmental issues. Among them, photocatalysis has attracted considerable attention for degrading organic pollutants in wastewater treatments by exploiting the energy from natural sunlight or artificial illumination.[6,7] Recently, synthesis of polymer-based photocatalysts has been extensively studied by the scientists owing to their extensive applications in multidisciplinary areas.[8,9] Among them, polyaniline (PANI) has been investigated comprehensively because of its unique conjugation mechanism, engaging benzenoid and quinoid rings escorting to three different oxidation states.[10] Moreover, PANI has been proved as a potential candidate in commercial applications owing to its large absorption coefficient in a visible region, easy protonation reversibility, excellent redox properties, and good environmental stability.[11,12] Also, it can efficiently sensitize organic dyes because of its superior light and thermal stability ensuring the recycling of the photocatalyst.[13] In order to recycle effectively, another aspect which should be taken care of is the mechanical stability of the photocatalyst. This can be achieved

Received: April 20, 2018
Accepted: June 26, 2018
Published: July 13, 2018

DOI: 10.1021/acsomega.8b00765
ACS Omega 2018, 3, 7846−7855

Scheme 1. Synthesis of the Hierarchically Structured Ternary Composite NiO@PANI/RGO for MB Degradation

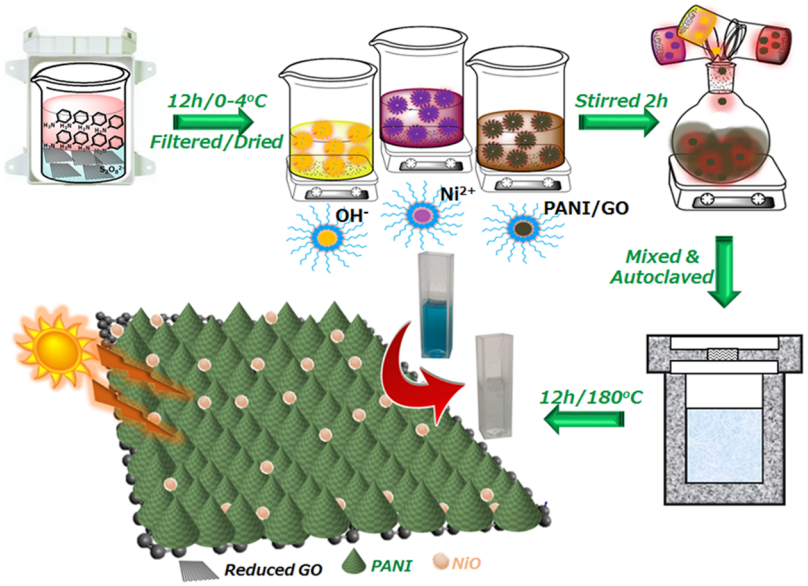

by offering a stable matrix, adding further to enhance the robustness of the resulting composite.

Graphene has emerged as a promising alternative because of its high surface area, zero band gap, and its ability to accept the electrons to prevent the recombination of photogenerated charge-carrying moieties.[14] Furthermore, it not only provides a two-dimensional (2D) plane for catalyst deposition but also enhances the adsorption capacity of the dye via $\pi-\pi$ conjugation between the dye and aromatic regions of graphene.[15−17] Furthermore, PANI acts as an electron donor and a hole conductor, whereas graphene acts as an electron acceptor on photoexcitation with visible or UV light.[18,19] Hence, their hybrid with inorganic materials or precisely transition-metal oxides additionally enhances the degradation rate owing to the synergistic effects by reducing recombination losses.[20,21] Different transition-metal oxides such as TiO_2, ZnO, MnO_2, nickel oxide (NiO), and Cu_2O have been investigated toward their photocatalytic activities.[22−24] Recently, researchers have shown an increasing interest toward the fabrication of a reduced graphene oxide (RGO)-based ternary composite, which can uniquely bring a synergistic effect. Miao et al. synthesized an RGO/PANI/Cu_2O hydrogel showing Congo red degradation in 20 min, signifying an improved performance of the composite.[20] Further, in situ polymerization of aniline with graphene and $ZnFe_2O_4$ results in a catalyst with augmented degradation efficiency for rhodamine B.[21] The composite of poly(3,4-ethylenedioxythiophene) (PEDOT) with graphene and MnO_2 by Zhang et al. also showed its catalytic activity by degrading methylene blue (MB) after 7 h.[1] Kumar et al. synthesized the PANI@TiO_2/GN photocatalyst for MB degradation within 180 min.[25] Variation in mechanical support by utilizing graphitic carbon nitride is also explored by Pendiselvi et al. for MB degradation, which took 80 min.[26] In addition, gold nanoparticles are also investigated in the ternary composite constituting graphene and TiO_2 for MB degradation, which demonstrates a complete MB degradation after 250 min.[27] Although significant milestones have been achieved, fabricating a hierarchically engineered ternary nanocomposite by optimizing material arrangement and taking advantage of their synergistic functions[28−30] with an outstanding activity remains a challenge. Furthermore, most of these photocatalysts are associated with drawbacks related to the low photoresponse of TiO_2 toward visible light, high cost of Ag or Au, which act as a prime element in the composites, and long degradation time.[31] Nevertheless, NiO nanopowder, an inexpensive, nontoxic, p-type semiconductor, with a wide band gap (3.2−3.8 eV) possessing unique electrochemical, catalytic, and magnetic properties with high hole mobility,[32] which can be synthesized in diverse morphologies using a facile synthetic method, has not found deserving attention.[33]

Following the above discussion, we have synthesized the hierarchical architecture of NiO (10 nm) nanoparticles adsorbed on the PANI nanospines (50−60 nm) uniformly grown on 2D RGO nanosheets (NiO@PANI/RGO) via a facile interfacial method, followed by a microemulsion solvothermal process. The as-prepared nanocomposite is evaluated using various microscopic and spectroscopic techniques to determine its physical and chemical properties. Furthermore, the photocatalytic activity along with the kinetics of degradation of MB illustrates the ultrafast catalytic activity with an enhanced cycling performance of the NiO@PANI/RGO composite.

2. RESULTS AND DISCUSSION

2.1. Preparation of a Hierarchical Nanocomposite.

The synthesis of the hierarchical nanocomposite NiO@PANI/RGO is schematically shown in Scheme 1. First, the PANI/GO composite was prepared by interfacial polymerization. GO prepared by modified Hummer's method along with oxidant ammonium peroxydisulfate (APS) was suspended in (0.1 M HCl) aqueous solution, while the monomer aniline dissolved in *n*-hexane formed the organic phase. The aniline monomer at the liquid/liquid interface (water/*n*-hexane) slowly diffuses from the organic phase to the aqueous phase where the oxygen functional groups on the GO surface act as the nucleation sites for polymerizing aniline to form uniform PANI nanospines. The presence of acidic aqueous medium facilitates the growth of a homogeneous composite exhibiting an intercalated PANI and GO structure instead of an individually grown

DOI: 10.1021/acsomega.8b00765
ACS Omega 2018, 3, 7846−7855

agglomerated form.[34] PANI/GO so formed acted as the matrix for the growth of NiO nanospheres on its surface by a microemulsion solvothermal method. In the microemulsion process, sodium sulfosuccinate (AOT)/isooctane, the nonpolar phase, forms reverse micelles having nanosized aqueous pools stabilized by the surfactant. These individual aqueous pools of PANI/GO, nickel chloride, and sodium hydroxide were mixed sequentially to make their micellar solutions and precipitated further under the solvothermal condition to give a hierarchical ternary composite (NiO@PANI/RGO).

2.2. Morphology and Structure. The surface morphologies of the RGO, PANI, PANI/RGO, and NiO@PANI/RGO composites were investigated using scanning electron microscopy (SEM) and transmission electron microscopy (TEM). Figure 1a,b shows the SEM images of the as-prepared RGO

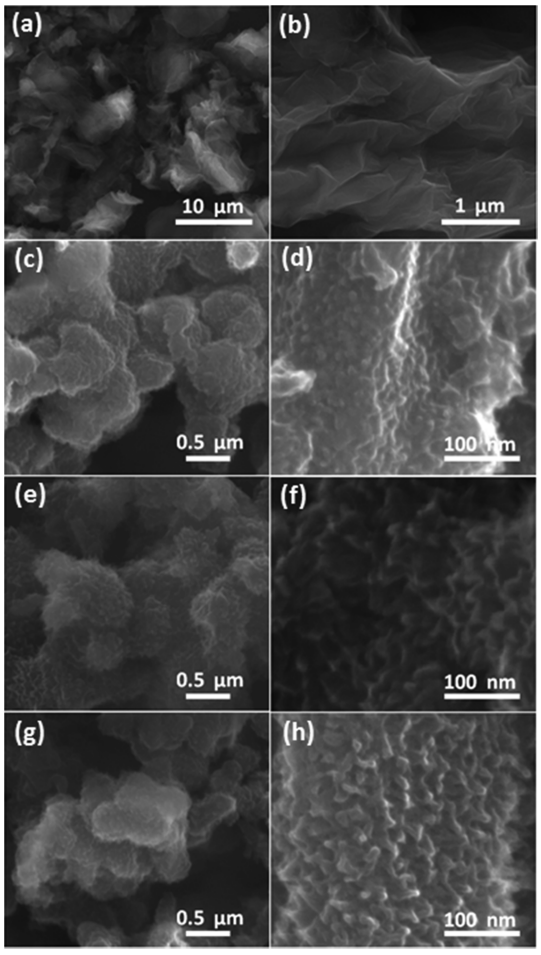

Figure 1. SEM micrographs of RGO (a,b), PANI (c,d), PANI/RGO (e,f), and NiO@PANI/RGO (g,h).

exhibiting a typical crumpled and wrinkled multilayered sheet structure with the size in tens of micrometers. PANI prepared by the interfacial method shows a globular cluster morphology (few micrometers) with uniformly grown 20−30 nm sized spines on its surface (Figure 1c,d). The morphology of PANI/RGO shown in Figure 1e,f is not much different from that of bare PANI, that is, the graphene surfaces are homogeneously covered with interconnected networks of PANI spines giving much higher loadings of PANI in the composite. However, an increase in the size of PANI spine to 50−60 nm is observed for PANI/RGO. This may be due to the presence of oxygen-containing functional groups on the GO surface, which act as the nucleation and growth sites for the PANI spines on the graphene matrix. These functional groups not only act as active sites but also minimize the interfacial energy barrier at the solid surface and bulk solution interface, resulting in an advantageous growth of the PANI spines.[29,35−37] The morphology of PANI/RGO is retained even after the formation of the NiO nanoparticles (Figure 1g,h). Because of the fine nature of NiO nanoparticles, they are either adsorbed on the exposed surfaces of PANI/RGO or intercalated between them. These NiO nanoparticles can be clearly seen from the TEM micrographs of NiO@PANI/RGO (Figure 2). The TEM image of RGO

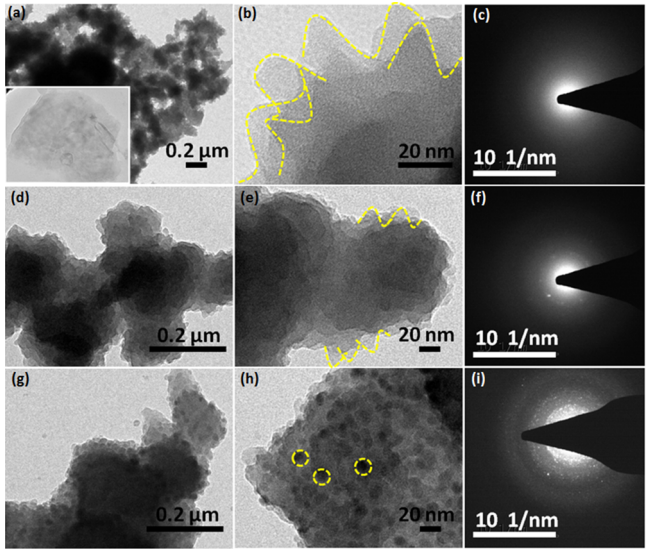

Figure 2. TEM (a,b,d,e,g,h) and SAED patterns (c,f,i) of PANI, PANI/RGO, and NiO@PANI/RGO, respectively. The inset in (a) shows the micrograph of RGO.

(inset, Figure 2a) demonstrates the exfoliated individual sheet structure, whereas bare PANI and PANI/RGO micrographs are dominated by the spines of PANI (Figure 2a,b,d,e, respectively). The selected area electron diffraction (SAED) patterns of bare PANI and PANI/RGO (Figure 2c,f) disclose that these materials lack the crystalline character. In contrast, the NiO@PANI/RGO micrographs shown in Figure 2g,h illustrate the homogeneously distributed NiO nanoparticles on the PANI/RGO surface. The spotty SAED pattern (Figure 2i) also demonstrates the nanocrystalline features of NiO. The average particle size, calculated from particle size distribution histogram, is found to be 10 nm for NiO. For further study, the high-resolution TEM (HRTEM) micrographs and 2D fast Fourier transform (2D FFT) images are taken (Figure 3) from the yellow colored circular portions in Figure 2h. Three distinctive sets of lattice fringes, which correspond to the 200, 111, and 220 planes having the *d*-spacing 0.2, 0.24, and 0.14 nm of NiO, are identified using HRTEM (Figure 3a−d), which also shows the correlation with 2D FFT calculations shown by Figure 3e.[38,39] Further, a higher Brunauer−Emmett−Teller surface area of NiO@PANI/RGO is achieved as compared to that of PANI and PANI/RGO (Figure S1) and found to be 90 m^2/g.

The powder X-ray diffractogram of NiO@PANI/RGO can be indexed to the NiO bunsenite structure (space group = *Fm3m* (225), JCPDS card #047-1049). As shown in Figure 4a,

DOI: 10.1021/acsomega.8b00765
ACS Omega 2018, 3, 7846−7855

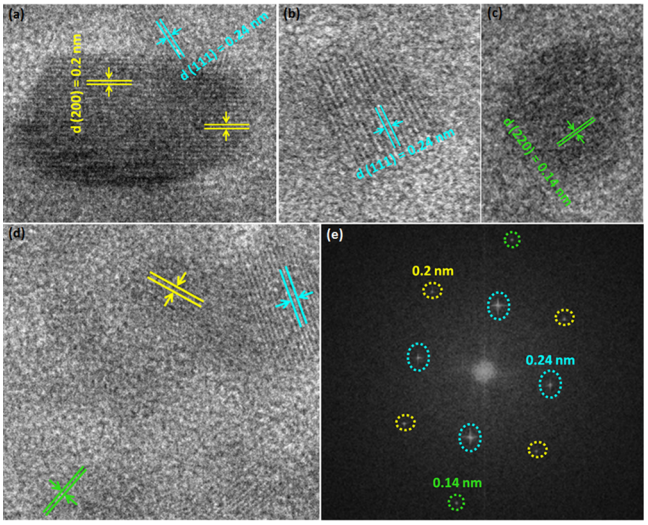

Figure 3. HRTEM micrographs (a–d) and the 2D FFT pattern (e) of NiO@PANI/RGO.

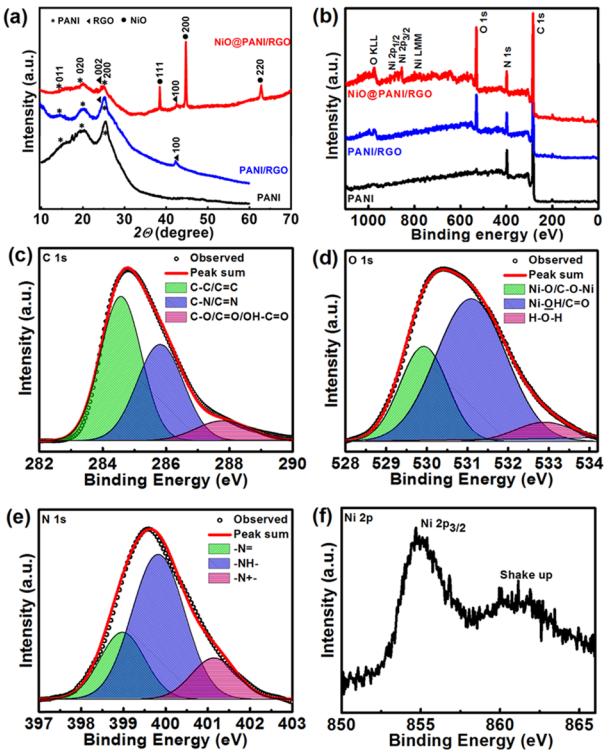

Figure 4. XRD pattern (a) and survey XPS spectra (b) of PANI, PANI/RGO, and NiO@PANI/RGO; the core XPS spectra of C 1s (c), O 1s (d), N 1s (e), and Ni 2p (f) of NiO@PANI/RGO.

the characteristic X-ray diffraction (XRD) peaks located at 2θ: 38.3, 44.5, and 66.2 correspond to the 111, 200, and 220 planes of NiO.[40] Absence of any other NiO phases confirms the high purity of the synthesized composite, NiO@PANI/RGO. The average crystallite size as calculated by the Scherrer formula is found to be ~7.0 nm,[41] which shows close resemblance to the particle size as observed by the HRTEM micrograph. Moreover, the XRD pattern also gives additional information regarding the presence of PANI and reduction of GO in the composite. Bare PANI demonstrates broad peaks, centered at 2θ = 15, 20.12, and 25.26°, and the same are also observed for binary and ternary composites as well. The XRD pattern of PANI/RGO reveals the characteristic reflection peaks for both PANI (at 2θ = 15, 20.12, and 25.26°) and RGO (at 2θ = 24.6, and 42.5°), indicating the successful polymerization of PANI on graphene. Furthermore, the NiO@PANI/RGO diffractogram exhibits the reflection peaks of PANI along with NiO. The peak at 2θ = 24.6° corresponding to the interlayer spacing of the graphene sheets overlaps with the broad diffraction of PANI, resulting in a broad peak around the 2θ value of ~25°.[34] The interaction of PANI and graphene is further ascertained by the Raman shift of the G peak in PANI/RGO and ternary composite as compared to RGO (Figure S2).

The surface composition and chemical states of the synthesized materials are analyzed by X-ray photoelectron spectroscopy (XPS), and the results are presented in Figure 4b–f. Figure 4b shows the survey spectra of PANI, PANI/RGO, and NiO@PANI/RGO. The presence of different elements C 1s, O 1s, N 1s, and Ni 2p is indexed in the figure. The core spectra of C 1s, O 1s, N 1s, and Ni 2p are deconvoluted using a Gaussian fitting method. Figure 4c displays the deconvoluted C 1s spectrum of NiO@PANI/RGO, revealing the presence of three different types of carbon functional groups, that is, nonoxygenated carbon (C–C/C═C/C–H) at 284.6 eV, oxygenated carbon (C–O/C═O/O–C═O) in the range 288 eV, and nitrogenated carbon (C–N/C═N) near 286.8 eV.[6] The comparative O 1s spectrum shows two peaks at 529.2 and 531.2 eV because of the Ni–O bond in NiO along with a peak at 533.5 eV (Figure 4d) attributed to the physisorbed and chemisorbed water and a number of surface species including hydroxyls, chemisorbed oxygen, and coordinated lattice oxygen for NiO@PANI/RGO.[42,43] The PANI/RGO O 1s core spectrum possesses peaks corresponding to only oxygen functionalities and chemisorbed or physisorbed water (Figure S3). The core N 1s spectrum of NiO@PANI/RGO (Figure 4e) illustrates three peaks corresponding to three different electronic states of nitrogen: the quinoid amine at 398.2 eV, the benzenoid amine at 399.4 eV, and the diminished nitrogen cationic radical ($N^{+\bullet}$) at 401 eV.[34] These observations indicate that PANI is in protonated state in the ternary composite and in all other synthesized samples under discussion. Figure 4f shows the Ni $2p_{3/2}$ spectrum centered around 854.5 eV with a shake-up peak at the high binding energy side of Ni $2p_{3/2}$, signifying the formation of NiO. Such a shake-up peak in the Ni XPS spectrum of NiO@PANI/RGO is attributed to arise from multiplet coupling and monopole charge-transfer transition (O 2p → Ni 3d).[44]

The variation in optical absorbance is examined using UV–vis spectroscopy (Figure S4). As compared to PANI and PANI/RGO, NiO@PANI/RGO shows optical absorption in the entire visible region, ascertaining that it could be utilized as efficient light absorbers with augmented photocatalytic properties. The optical band gap of PANI as calculated by the Tauc plot (Figure S4) is found to be 2.6 eV, whereas the in situ introduction of graphene in PANI decreases the band gap by 0.3 eV for PANI/RGO. Furthermore, in the case of the ternary composite, the band gap decreased to 1.9 eV, which ascertains our proposal of making ternary nanocomposites for effective sunlight utilization.

Such uniformly distributed NiO nanoparticles over PANI spines grown on the RGO surface in the hierarchical mode with an optimum band gap are expected to show strong synergistic interactions, resulting in an enhanced photocatalytic activity of the ternary composite NiO@PANI/RGO.

DOI: 10.1021/acsomega.8b00765
ACS Omega 2018, 3, 7846–7855

2.3. Photocatalytic Evaluation. The graphene nanocomposite-based photocatalysis is widely employed as a potential approach for decomposing environmental hazardous materials owing to their wide spectral range of irradiation. MB, a chemically stable dye, is considered as an organic pollutant[45] and used to investigate the photocatalytic performance of NiO@PANI/RGO by scrutinizing its degradation in an aqueous solution. Blank tests performed in the presence of light and $NaBH_4$ show insignificant degradation even after 60 min of treatment as can be observed from Figure 5a. This

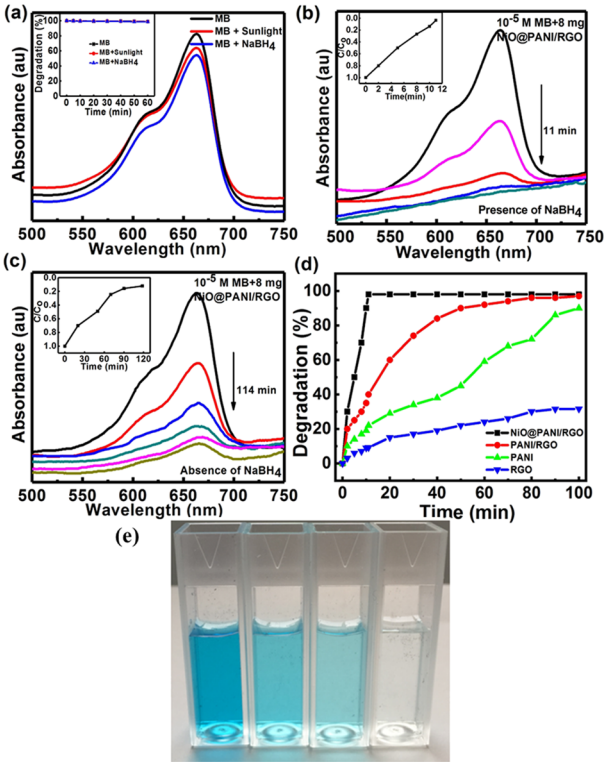

Figure 5. (a) UV−vis spectra of MB degradation (10^{-5} M) in dark and in the presence of sunlight and $NaBH_4$; the inset shows the degradation of MB after 100 min in the three cases. (b,c) UV−vis spectra of MB degradation in the presence of NiO@PANI/RGO with and without $NaBH_4$, respectively. The inset shows their respective C/C_0 vs time plots. (d) Comparative degradation efficiency of ternary (NiO@PANI/RGO), binary (PANI/RGO), bare PANI, and RGO and (e) digital image of MB degradation in the presence of the NiO@PANI/RGO photocatalyst (0 min → 4 min → 8 min → 11 min).

indicates that MB degradation is negligible without adding the photocatalyst (inset, Figure 5a), revealing the importance of the catalyst for an effective mineralization of the dye molecules. Besides, the experimental result confirms that the MB aqueous solution is highly stable and dormant under visible light.

Figure 5b,c shows a variation in the UV−vis spectra during MB degradation in the presence of the NiO@PANI/RGO catalyst with and without $NaBH_4$, respectively. The characteristic absorbance of MB at 664 nm[7] decreases rapidly as the time prolonged and the solution eventually turned colorless [leuco MB (LMB)], as shown by temporal evolution of the MB degradation process in Figure 5e. The time taken by the ternary composite in degrading MB (∼65%) in the absence of $NaBH_4$ is very less as compared to the degradation (∼98%) in the presence of $NaBH_4$. This can be attributed to the relay effect of the ternary composite in which the nanoparticles act as an electron relay and commence the shifting of electron from BH_4^- [donor (B_2H_4/BH_4^-)] to MB [acceptor (LMB/MB)] and thus result in the reduction of the dye (Figure S5). The in situ BH_4^- formed get simultaneously adsorbed on the surface of the ternary composite and thus electron transfer occurs from BH_4^- to MB through the NiO@PANI/RGO composite, making the dye colorless after reduction.[46−48] The active species during the degradation process is also analyzed by scavenging experiments[7] and shown in Figure S6. It is clearly noted from the figure that degradation is affected by the addition of different scavengers in the presence of NiO@PANI/RGO + $NaBH_4$. However, in the degradation process with different scavengers, the degree of MB degradation decreases to 78, 75, and 37% with the addition of ammonium oxalate, isopropyl alcohol (IPA), and methanol (MeOH) (Figure S6), implying that $O_2^{-\bullet}$ is the dominating active radical in the MB decomposition process in the presence of NiO@PANI/RGO + $NaBH_4$, thereby resulting in an ultrafast sunlight-driven degradation of MB.

In order to compare the performance, NiO@PANI/RGO, PANI/RGO, bare PANI, and RGO are explored as photocatalysts under similar experimental conditions. It is interesting to note that MB degradation in the presence of NiO@PANI/RGO takes ∼11 min for almost complete degradation (∼98%), whereas PANI/RGO, PANI, and RGO take an extended time duration to degrade 97, 84, and 32% of MB, respectively, revealing the ultrafast degradation by NiO@PANI/RGO (Figure 5d). The difference in the photocatalytic rates may attribute to the interaction of MB molecules with PANI, NiO, and RGO, affecting their adsorption on the composite surface. Improved adsorption takes place on the hierarchically fabricated ternary composite owing to its enhanced active surface sites with an augmented interface charge-transfer efficiency, which is further analyzed by electrochemical impedance spectroscopy (EIS). In the EIS Nyquist plot, the radius of the arc in the high-frequency region (inset) (charge-transfer resistance, R_{CT} as in Figure S7b) reflects the reaction rate occurring on the surface of the electrode.[17] PANI shows an R_{CT} of 3.1 Ω, which decreases to 0.8 Ω by introducing RGO in PANI, enhancing the effective separation of photogenerated carriers. Compared with PANI and PANI/RGO, the ternary composite (NiO@PANI/RGO) possesses the lowest value of R_{CT}, 0.3 Ω, indicating an augmented separation efficiency of the photogenerated electron−hole pairs and faster interfacial charge-transfer rates in accordance with the displayed results of MB degradation.

In order to determine the specific amount of the dye concentration, experiments were carried out by varying different concentrations of the MB dye (10^{-4} and 10^{-3} M) (Figure 6a,b) by using 8 mg of the catalyst (NiO@PANI/RGO). Their insets demonstrate the time course of C/C_0. Further, in order to evaluate the kinetic mechanism of degradation of MB using the NiO@PANI/RGO ($NaBH_4$) photocatalyst, the degradation results are examined according to first-order kinetics (Figure 6c):

$$\text{First-order kinetic: } \ln(C_0/C_t) = k_1 t$$

where C_0 is the initial concentration of MB solution, C_t is the concentration of the MB solution after treatment at time t, and k_1 is first-order rate constant.[49]

The degradation of MB follows a first-order kinetic model as shown by its regression coefficient ($R^2 > 0.99$). As the concentration of MB changes from 10^{-5} to 10^{-3} M, the

DOI: 10.1021/acsomega.8b00765
ACS Omega 2018, 3, 7846−7855

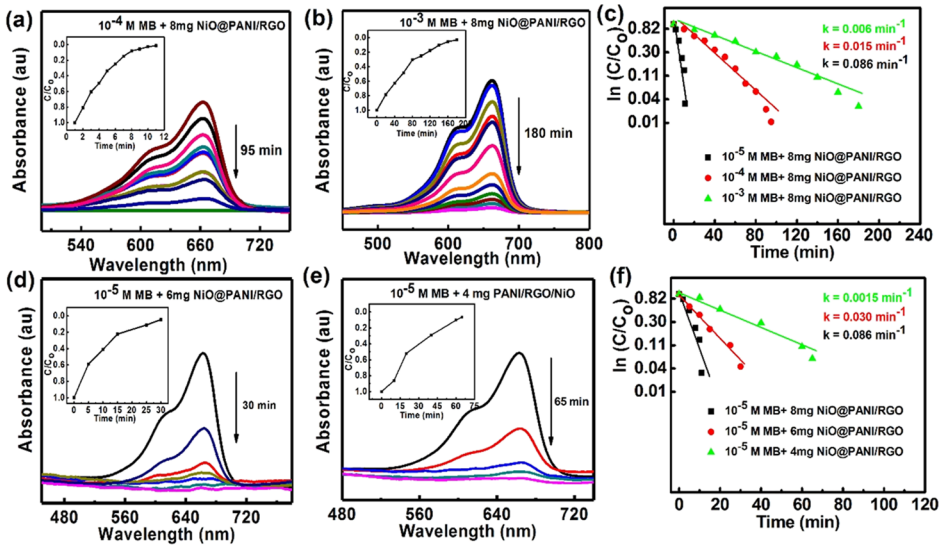

Figure 6. UV−vis spectra for MB degradation (a) 10^{-4} M and (b) 10^{-3} M in the presence of 8 mg NiO@PANI/RGO photocatalyst. The inset shows their respective C/C_0 vs time plots, (c) plot of $\ln(C/C_0)$ vs time to analyze the kinetics; UV−vis spectra for MB degradation in the presence of NiO@PANI/RGO (d) 6 mg and (e) 4 mg. The inset shows their respective C/C_0 vs time plots and (f) plot of $\ln(C/C_0)$ vs time to analyze the kinetics with different concentrations of the photocatalyst.

reaction rate constant (k) decreases, that is, 0.086, 0.015, and 0.006 min^{-1}, respectively. With an increasing concentration, the decrement in the rate constant may be attributed to the excess of MB molecules getting adsorbed on the catalyst surface.

Furthermore, the photocatalyst concentration is varied (4−8 mg in 30 mL of MB solution; 10^{-5} M), and the result toward the MB degradation process is further explored (Figure 6d,e for 6 and 4 mg photocatalyst, respectively). It is observed that the decolorization efficiency is highest with 8 mg photocatalyst with the rate constant of 0.086 min^{-1} (Figure 6f), which can be attributed to higher available active sites of the photocatalyst. However, a further increment in the photocatalyst amount (10 mg) decreases the degradation rate (not shown here). This may attribute to the aggregation of the nanocomposite, resulting in decreased active sites at a higher concentration. Hence, the photocatalyst amount was kept as 8 mg (else specified) in the subsequent analysis for obtaining maximum degradation efficiency.

The recyclability of the photocatalyst (NiO@PANI/RGO) is further analyzed by its repeated use toward the catalytic activity. Ten rounds of degradation reaction for MB (10^{-5} M) are accomplished with the recycling of the catalyst under the same reaction condition (Figure 7). After the completion of the first cycle, the photocatalyst was washed with double-distilled water and dried prior to the next use. The results in 3D representation (Figure 7a) demonstrated that NiO@PANI/RGO maintained a consistent activity even after 10 runs of the catalyst. The slight demur of the degradation degree (Figure 7b) may be attributed to the loss of the catalyst during the recovery process. In addition, the good reliability and stability of the NiO@PANI/RGO catalyst are also confirmed by the XRD measurements of the catalyst, before and after the degradation cycles (Figure 7c). As compared to the fresh catalyst, no significant change in the XRD patterns is observed, suggesting an excellent stability of the photocatalyst (NiO@PANI/RGO) during MB degradation.

The photocatalytic performance of NiO@PANI/RGO in comparison with that of the other recently reported ternary

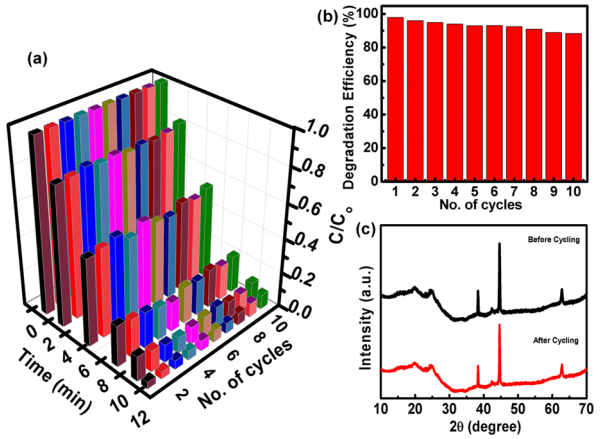

Figure 7. (a) 3D representations of 10 cycling scans for MB degradation by NiO@PANI/RGO, (b) variation in the degradation efficiency of the ternary catalyst during 10 degradation cycles, and (c) XRD profile of NiO@PANI/RGO, before and after the degradation cycle.

composites is presented in Table 1. It is observed from the table that the hierarchically structured NiO@PANI/RGO photocatalyst is much superior compared to the previously reported catalysts for sunlight-driven MB degradation. Furthermore, the hierarchical NiO@PANI/RGO photocatalyst presented in this work requires a very short degradation time with a significantly small amount bestowing a persuasive sunlight-driven photocatalyst for MB removal.

3. CONCLUSIONS

To summarize, the hierarchical structured ternary composite (NiO@PANI/RGO) with a higher adsorption ability has been synthesized by interfacial polymerization, followed by a microemulsion solvothermal process. The morphology characterization results ascertain the formation of the NiO nanoparticles (10 nm) over the PANI spines (50−60 nm) grown uniformly over the 2D graphene sheets. The NiO@PANI/RGO composite formed acts as an efficient photo-

DOI: 10.1021/acsomega.8b00765
ACS Omega 2018, 3, 7846−7855

Table 1. Comparative Data of Photocatalytic Activity of Various Ternary Composites for MB Degradation

s. no.	photocatalyst	catalyst amount (mg)	% degradation	concn of dye (MB)	time (min)	references	light condition
1	PEDOT/GO/MnO_2	20	92.7	50 mL	420	56	sunlight
2	PANI@GN/TiO_2	50	87	100 mL of 10.5 mg/L	180	25	
3	Ag_2O/TiO_2@PPY	50	100	100 mL of 20 mg/L	240	57	visible light (104 W)
4	RGO−Fe_3O_4−TiO_2	50	91	100 mL of 1 mg/L	5	58	white phosphor coated bulb
5	CN−NS/PANI/ZnO	5		10 mL of 60 μL of 0.2% sol	80	26	300 W halogen lamp
6	RGO/mesoTiO_2/AuNP	10		70 mL of 30 mg/L	240	27	500 W halogen tungsten lamp
7	Ag−Ag_2O/TiO_2@PPY	100	∼100	100 mL of 4 mg/L	175	59	visible light (112 W)
8	Pd−TiO_2−$SrIn_2O_4$	100	∼90	100 mL of 50 ppm	50	60	sun light
9	**NiO@PANI/RGO**	**8**	**98%**	**30 mL of 10^{-5} M**	**11**	**this work**	**sun light**

catalyst for MB dye degradation under sunlight irradiation. The NiO@PANI/RGO photocatalyst can rapidly degrade 98% of the MB aqueous solution (10^{-5} M) in 11 min following the first-order reaction at a rate constant of 0.086 min^{-1}. This enhanced photocatalytic activity is ascribed to the synergistic effect of an increased lifetime of photoexcited charge carriers in the hierarchical nanocomposite. In addition to this, increasing the concentration of the photocatalyst has a significant effect on the rate constant of MB degradation because of the increasing availability of adsorption and photocatalytic centers. Moreover, the NiO@PANI/RGO composite is found to perform a rapid MB degradation compared to PANI/RGO and bare PANI. Furthermore, the photocatalyst preserves an ultrafast and repetitive degradation efficiency up to 5 MB degradation cycles and maintains an 89% efficiency even after 10 degradation cycles. Thus, the development of such hierarchical metal oxide/polymer/graphene composites by the facile synthesis method represents a very stable, recyclable, and economical approach for the degradation of highly dangerous MB dyes in the wastewater.

4. EXPERIMENTAL DETAILS

4.1. Materials and Methods. Graphite powders (CAS no. 7782-42-5, particle size <45 μm, 99.99% purity) were obtained from Aldrich Chemicals Inc. Nickel chloride ($NiCl_2·4H_2O$), aniline, sodium hydroxide (NaOH), sodium borohydride ($NaBH_4$), APS, IPA, isooctane, sodium sulfate (Na_2SO_4), and hydrochloric acid (HCl) were of GR grade and were used as received from Merck. AOT was used as the surfactant (supplied by Alfa Aesar).

The as-prepared samples were characterized by a field emission scanning electron microscope (JEOL, JXA-8230) at an accelerating voltage of 10 kV, a high-resolution transmission electron microscope (FEI Tecnai G2 12 Twin TEM operating at 120 kV), the powder XRD measurements (an X'Pert Pro MPD X-ray diffractometer) employing monochromatized Cu Kα radiation (λ = 1.54056 Å) at 298 K, an X-ray photoelectron spectrometer (PHI 5000 Versa Prob II, FEI Inc), and Raman spectroscopy on a Renishaw inVia Raman microscope equipped with a laser having a wavelength of 514 nm. The EIS analysis in a frequency range 1 mHz to 1 MHz was performed by CHI760 in a three-electrode assembly in 0.5 M Na_2SO_4. Platinum and Ag/AgCl were assembled as the counter and reference electrodes, respectively. Polished graphite (1 cm^2) coated with a synthesized material served as the working electrode. Further, a degradation study was performed using a UV−vis spectrometer (PE LAMBDA 650/850/950).

4.2. Preparation of PANI. PANI was prepared by a typical procedure via in situ chemical oxidative interfacial polymerization.[34] Briefly, aniline (0.5 M) was dissolved in 20 mL of precooled *n*-hexane solvent under vigorous stirring at room temperature. Separately, APS (2 M) (keeping the molar ratio of aniline/APS as 1:4) was dissolved in 20 mL of precooled 1 M HCl solution. Subsequently, the aniline monomer solution was added very slowly to the APS solution to form an immiscible liquid/liquid interface. The mixed solution was at a constant temperature 0−4 °C, and the polymerization was allowed to proceed at the interface for 12 h without stirring. Polymerization started within few minutes, which can be identified by the formation of green colored PANI (emeraldine salt) at the *n*-hexane/water interface. The polymerized product was separated by filtration using a cellulose nitrate membrane (0.45 μm) and washed with methanol to remove the oligomeric products. After washing with a copious amount of deionized water, the sample was dried in vacuum for 12 h.

4.3. Preparation of the PANI/GO Composite. GO was synthesized from graphite powder by modified Hummer's method.[50] The in situ chemical oxidative interfacial polymerization method was used for the synthesis of the PANI/GO composite following the similar procedure as that adopted for PANI synthesis with the exception that GO (the weight ratio of aniline to GO is 80:20) was also added along with APS in 1 M HCl aqueous solution and sonicated to form a homogeneous suspension. Thereafter, a precooled aniline monomer dissolved in *n*-hexane (molar ratio of aniline/APS 1:4) was slowly added into the above solution and kept constant for 12 h maintaining the temperature at 0−4 °C. The resulting product was filtered using a cellulose nitrate membrane (0.45 μm) and washed with methanol and deionized water. Finally, the powdery composite PANI/GO was dried at 60 °C for 12 h in vacuum and used for synthesizing a ternary composite with NiO.

4.4. Preparation of the NiO, PANI, and RGO Ternary Composite (NiO@PANI/RGO). The NiO@PANI/RGO composite was synthesized using the microemulsion method. At first, the microemulsion solutions were prepared by taking AOT in isooctane, which acts as the organic phase. Nickel chloride ($NiCl_2$) and precipitating agent (NaOH) dissolved in water acted as the aqueous phase. Typically, 6 g AOT was dissolved in 60 mL of isooctane and divided into three parts of 20 mL each.[51−53] Afterward, 20 mL aqueous solutions of 0.5 M $NiCl_2$, 2 M NaOH, and 20 wt % PANI/GO were added to the AOT/isooctane solutions, respectively. Each of these microemulsions was stirred for 2 h. The resulting solutions were mixed together in a reaction vessel, transferred to an autoclave, and kept at 180 °C for 12 h, followed by natural

DOI: 10.1021/acsomega.8b00765
ACS Omega 2018, 3, 7846−7855

cooling. The as-obtained black precipitate was filtered and washed with deionized water, followed by drying at 60 °C in vacuum.[54] Also, graphene oxide in the composite was reduced to graphene during the in situ growth of NiO.[51] The resulting powder was dispersed in 10 mL of 0.1 M HCl solution and stirred at room temperature overnight to obtain NiO@PANI/RGO. The final composite was filtered, washed, and dried at 60 °C in vacuum. The dried NiO@PANI/RGO powder was used for characterization and photocatalytic activity. The ratio of wt % of individual components RGO/PANI/NiO in the ternary composite (NiO@PANI/RGO) is 4:16:80, as calculated by the reactants taken in the initial synthesis stage. For comparison, PANI/RGO was also prepared following the similar reduction process.

4.5. Photocatalytic Experiment. The photocatalytic activity of the prepared samples was determined based on the sunlight-driven degradation of MB. In a typical experiment, the photocatalyst (8 mg) was mixed with the MB solution (10^{-5} M), which was further stirred in dark for 30 min to reach the adsorption equilibrium prior to the photocatalytic test. Then, fresh aqueous $NaBH_4$ (0.01 M) was mixed in the above solution, followed by irradiation with solar light. These experiments were conducted in October between 11 am and 12 pm. After a particular interval, 2 mL aliquot was sampled and the change in MB concentration was estimated by a UV−vis spectrophotometer. The experiments were done in triplicate to achieve reliable results. The photocatalytic activities of the samples were evaluated by measuring the decolorization efficiency (%) of the MB solution.

The reproducibility of the photocatalytic degradation activity on the NiO@PANI/RGO nanocomposite was studied at a constant MB concentration (10^{-5} M) and a catalyst dosage of 8 mg in 30 mL dye solution in each cycle. The recovered catalyst was washed with ethanol and deionized water, followed by drying before its reuse in the next photocatalytic cycle.

The degree of degradation (%) is calculated by using the relation[54]

$$D = \frac{C_0 - C_t}{C_0} \times 100$$

where C_0 and C_t are the initial and remaining concentrations of MB at different times, respectively. C_0/C can be substituted by A_0/A for the reason that the concentration (C) is directly proportional to the absorbance (A) as

$$C_t = kA_t$$

where k is a constant and A is the absorption intensity.[55]

■ ASSOCIATED CONTENT

Supporting Information

The Supporting Information is available free of charge on the ACS Publications website at DOI: 10.1021/acsomega.8b00765.

Thermogravimetric analysis; N_2 adsorption−desorption isotherm; XPS, EIS, and UV−vis spectra of the related materials with the role of $NaBH_4$ (the relay effect); and degradation mechanism with and without scavengers (PDF)

■ AUTHOR INFORMATION

Corresponding Author

*E-mail: shamim_chem@yahoo.co.in (M.S.).

ORCID

Mohammed Samim: 0000-0003-1667-8572

Notes

The authors declare no competing financial interest.

■ ACKNOWLEDGMENTS

P.A. acknowledges NPDF (project no. PDF/2015/000470) from the Department of Science and Technology, India. Special thanks to labmates, Mobin, Pankaj, and Khuntia Sir for their support in carrying out this work. Dr. Rajni Kanojia's support was highly acknowledged.

■ REFERENCES

(1) Grimm, N. B.; Faeth, S. H.; Golubiewski, N. E.; Redman, C. L.; Wu, J.; Bai, X.; Briggs, J. M. Global Change and the Ecology of Cities. *Science* **2008**, *319*, 756−760.

(2) Fahel, J.; Kim, S.; Durand, P.; André, E.; Carteret, C. Enhanced catalytic oxidation ability of ternary layered double hydroxides for organic pollutants degradation. *Dalton Trans.* **2016**, *45*, 8224−8235.

(3) Zhang, Y.; Park, M.; Kim, H. Y.; Ding, B.; Park, S.-J. In situ synthesis of nanofibers with various ratios of $BiOCl_x/BiOBr_y/BiOI_z$ for effective trichloroethylene photocatalytic degradation. *Appl. Surf. Sci.* **2016**, *384*, 192−199.

(4) Zhang, Y.; Park, S.-J. Au-pd bimetallic alloy nanoparticle-decorated $BiPO_4$ nanorods for enhanced photocatalytic oxidation of trichloroethylene. *J. Catal.* **2017**, *355*, 1−10.

(5) Amini, M.; Pourbadiei, B.; Purnima, T.; Ruberu, A.; Woo, L. K. Catalytic activity of MnO_x/WO_3 nanoparticles: synthesis, structure characterization and oxidative degradation of methylene blue. *New J. Chem.* **2014**, *38*, 1250−1255.

(6) Shahabuddin, S.; Sarih, N. M.; Ismail, F. H.; Shahid, M. M.; Huang, N. M. Synthesis of chitosan grafted-polyaniline/Co_3O_4 nanocube nanocomposites and their photocatalytic activity toward methylene blue dye degradation. *RSC Adv.* **2015**, *5*, 83857−83867.

(7) Yu, C.; Wang, K.; Yang, P.; Yang, S.; Lu, C.; Song, Y.; Dong, S.; Sun, J.; Sun, J. One-pot facile synthesis of $Bi_2S_3/SnS_2/Bi_2O_3$ ternary heterojunction as advanced double Z-scheme photocatalytic system for efficient dye removal under sunlight irradiation. *Appl. Surf. Sci.* **2017**, *420*, 233−242.

(8) Jiang, H.-Y.; Zhou, P.; Wang, Y.; Duan, R.; Chen, C.; Song, W.; Zhao, J. Copper based coordination polymer nanostructure for visible light photocatalysis. *Adv. Mater.* **2016**, *28*, 9776−9781.

(9) Li, J.; Xiao, Q.; Li, L.; Shen, J.; Hu, D. Novel ternary composites: Preparation, performance and application of $ZnFe_2O_4/TiO_2$/polyaniline. *Appl. Surf. Sci.* **2015**, *331*, 108−114.

(10) Reddy, K. R.; Karthik, K. V.; Prasad, S. B. B.; Soni, S. K.; Jeong, H. M.; Raghu, A. V. Enhanced photocatalytic activity of nanostructured titanium dioxide/polyaniline hybrid photocatalysts. *Polyhedron* **2016**, *120*, 169−174.

(11) Xiong, P.; Chen, Q.; He, M.; Sun, X.; Wang, X. Cobalt ferrite−polyaniline heteroarchitecture: a magnetically recyclable photocatalyst with highly enhanced performances. *J. Mater. Chem.* **2012**, *22*, 17485−17493.

(12) Ayad, M. M.; El-Nasr, A. A. Adsorption of cationic dye (methylene blue) from water using polyaniline nanotubes base. *J. Phys. Chem. C* **2010**, *114*, 14377−14383.

(13) Guo, N.; Liang, Y.; Lan, S.; Liu, L.; Zhang, J.; Ji, G.; Gan, S. Microscale hierarchical three-dimensional flowerlike TiO_2/PANI composite: synthesis, characterization, and its remarkable photocatalytic activity on organic dyes under UV-light and sunlight irradiation. *J. Phys. Chem. C* **2014**, *118*, 18343−18355.

(14) Dong, S.; Ding, X.; Guo, T.; Yue, X.; Han, X.; Sun, J. Self-assembled hollow sphere shaped Bi2WO6/RGO composites for

DOI: 10.1021/acsomega.8b00765
ACS Omega 2018, 3, 7846−7855

efficient sunlight-driven photocatalytic degradation of organic pollutants. *Chem. Eng. J.* **2017**, *316*, 778−789.
(15) Dong, S.; Cui, Y.; Wang, Y.; Li, Y.; Hu, L.; Sun, J.; Sun, J. Designing three-dimensional acicular sheaf shaped $BiVO_4$/reduced graphene oxide composites for efficient sunlight-driven photocatalytic degradation of dye wastewater. *Chem. Eng. J.* **2014**, *249*, 102−110.
(16) Yang, H.; Liu, X.; Sun, S.; Nie, Y.; Wu, H.; Yang, T.; Zheng, S.; Lin, S. Green and facile synthesis of graphene nanosheets/$K_3PW_{12}O_{40}$ nanocomposites with enhanced photocatalytic activities. *Mater. Res. Bull.* **2016**, *78*, 112−118.
(17) Yu, C.; Dong, S.; Zhao, J.; Han, X.; Wang, J.; Sun, J. Preparation and characterization of sphere-shaped BiVO4/reduced graphene oxide photocatalyst for an augmented natural sunlight photocatalytic activity. *J. Alloys Compd.* **2016**, *677*, 219−227.
(18) O'Mullane, A. P.; Dale, S. E.; Macpherson, J. V.; Unwin, P. R. Fabrication and electrocatalytic properties of polyaniline/Pt nanoparticle composites. *Chem. Commun.* **2004**, 1606−1607.
(19) Min, S.; Lu, G. Dye-sensitized reduced graphene oxide photocatalysts for highly efficient visible-light-driven water reduction. *J. Phys. Chem. C* **2011**, *115*, 13938−13945.
(20) Miao, J.; Xie, A.; Li, S.; Huang, F.; Cao, J.; Shen, Y. A novel reducing graphene/polyaniline/cuprous oxide composite hydrogel with unexpected photocatalytic activity for the degradation of Congo red. *Appl. Surf. Sci.* **2016**, *360*, 594−600.
(21) Feng, J.; Hou, Y.; Wang, X.; Quan, W.; Zhang, J.; Wang, Y.; Li, L. In-depth study on adsorption and photocatalytic performance of novel reduced graphene oxide-$ZnFe_2O_4$-polyaniline composites. *J. Alloys Compd.* **2016**, *681*, 157−166.
(22) Zhang, W.; Li, X.; Yang, Z.; Tang, X.; Ma, Y.; Li, M.; Hu, N.; Wei, H.; Zhang, Y. In situ preparation of cubic Cu_2O-RGO nanocomposites for enhanced visible- light degradation of methyl orange. *Nanotechnology* **2016**, *27*, 265703.
(23) Pajootan, E.; Arami, M.; Rahimdokht, M. Application of carbon nanotubes coated electrodes and immobilized TiO_2 for dye degradation in a continuous photocatalytic-electro-fenton process. *Ind. Eng. Chem. Res.* **2014**, *53*, 16261−16269.
(24) Raizada, P.; Singh, P.; Kumar, A.; Sharma, G.; Pare, B.; Jonnalagadda, S. B.; Thakur, P. Solar photocatalytic activity of nano-ZnO supported on activated carbon or brick grain particles: Role of adsorption in dye degradation. *Appl. Catal., A* **2014**, *486*, 159−169.
(25) Kumar, R.; Ansari, M. O.; Parveen, N.; Oves, M.; Barakat, M. A.; Alshahri, A.; Khan, M. Y.; Cho, M. H. Facile route to a conducting ternary polyaniline@TiO2/GN nanocomposite for environmentally benign applications: photocatalytic degradation of pollutants and biological activity. *RSC Adv.* **2016**, *6*, 111308−111317.
(26) Pandiselvi, K.; Fang, H.; Huang, X.; Wang, J.; Xu, X.; Li, T. Constructing a novel carbon nitride/polyaniline/ZnO ternary heterostructure with enhanced photocatalytic performance using exfoliated carbon nitride nanosheets as supports. *J. Hazard. Mater.* **2016**, *314*, 67−77.
(27) Yang, Y.; Ma, Z.; Xu, L.; Wang, H.; Fu, N. Preparation of reduced graphene oxide/meso-TiO_2/AuNPs ternary composites and their visible-light-induced photocatalytic degradation of methylene blue. *Appl. Surf. Sci.* **2016**, *369*, 576−583.
(28) Qian, H.; Greenhalgh, E. S.; Shaffer, M. S. P.; Bismarck, A. Carbon nanotube-based hierarchical composites: a review. *J. Mater. Chem.* **2010**, *20*, 4751−4762.
(29) Xu, J.; Wang, K.; Zu, S.-Z.; Han, B.-H.; Wei, Z. Hierarchical nanocomposites of polyaniline nanowire arrays on graphene oxide sheets with synergistic effect for energy storage. *ACS Nano* **2010**, *4*, 5019−5026.
(30) Ujjain, S. K.; Roy, P. K.; Kumar, S.; Singha, S.; Khare, K. Uniting superhydrophobic, superoleophobic and lubricant infused slippery behavior on copper oxide nano-structured substrates. *Sci. Rep.* **2016**, *6*, 35524.
(31) Raghavan, N.; Thangavel, S.; Venugopal, G. Enhanced photocatalytic degradation of methylene blue by reduced graphene-oxide/titanium dioxide/zinc oxide ternary nanocomposites. *Mater. Sci. Semicond. Process.* **2015**, *30*, 321−329.
(32) Wang, M.; Hu, Y.; Han, J.; Guo, R.; Xiong, H.; Yin, Y. TiO_2/NiO hybrid shells: p−n junction photocatalysts with enhanced activity under visible light. *J. Mater. Chem. A* **2015**, *3*, 20727−20735.
(33) Chen, W. X.; Yu, J. S.; Hu, W.; Chen, Z. L.; Memon, H.; Chen, G. L. Titanate nanowire/NiO nanoflake core/shell heterostructured nanonanocomposite catalyst for methylene blue photodegradation. *RSC Adv.* **2016**, *6*, 67827−67832.
(34) Zhang, K.; Zhang, L. L.; Zhao, X. S.; Wu, J. Graphene/Polyaniline nanofiber composites as supercapacitor electrodes. *Chem. Mater.* **2010**, *22*, 1392−1401.
(35) Vivekchand, S. R. C.; Rout, C. S.; Subrahmanyam, K. S.; Govindara, A.; Rao, C. N. R. Graphene-based electrochemical supercapacitors. *J. Chem. Sci.* **2008**, *120*, 9−13.
(36) Chiou, N.-R.; Lu, C.; Guan, J.; Lee, L. J.; Epstein, A. J. Growth and alignment of polyaniline nanofibres with superhydrophobic, superhydrophilic and other properties. *Nat. Nanotechnol.* **2007**, *2*, 354−357.
(37) de Oliveira, H. P.; Sydlik, S. A.; Swager, T. M. Supercapacitors from free-standing polypyrrole/graphene nanocomposites. *J. Phys. Chem. C* **2013**, *117*, 10270−10276.
(38) Su, D.; Ford, M.; Wang, G. Mesoporous NiO crystals with dominantly exposed {110} reactive facets for ultrafast lithium storage. *Sci. Rep.* **2012**, *2*, 924.
(39) Ghosh, M.; Biswas, K.; Sundaresan, A.; Rao, C. N. R. MnO and NiO nanoparticles: synthesis and magnetic properties. *J. Mater. Chem.* **2006**, *16*, 106−111.
(40) Long, H.; Shi, T.; Hu, H.; Jiang, S.; Xi, S.; Tang, Z. Growth of hierarchal mesoporous NiO nanosheets on carbon cloth as binder-free anodes for high-performance flexible lithium-ion batteries. *Sci. Rep.* **2014**, *4*, 7413.
(41) Subramanian, E.; Subbulakshmi, S.; Murugan, C. Inter-relationship between nanostructures of conducting polyaniline and the photocatalytic methylene blue dye degradation efficiencies of its hybrid composites with anatase TiO_2. *Mater. Res. Bull.* **2014**, *51*, 128−135.
(42) Liu, W.; Lu, C.; Wang, X.; Liang, K.; Tay, B. K. In situ fabrication of three-dimensional, ultrathin graphite/carbon nanotube/NiO composite as binder-free electrode for high-performance energy storage. *J. Mater. Chem. A* **2015**, *3*, 624−633.
(43) Ju, Z.; Ma, G.; Zhao, Y.; Xing, Z.; Qiang, Y.; Qian, Y. A Facile Method for Synthesis of Porous $NiCo_2O_4$ Nanorods as a High-Performance Anode Material for Li-Ion Batteries. *Part. Part. Syst. Charact.* **2015**, *32*, 1012−1019.
(44) Kim, K. S.; Winograd, N. X-Ray Photoelectron spectroscopic studies of nickel-oxygen surfaces using oxygen and argon ion-bombardment. *Surf. Sci.* **1974**, *43*, 625−643.
(45) Nath, S.; Ghosh, S. K.; Panigahi, S.; Thundat, T.; Pal, T. Synthesis of selenium nanoparticle and its photocatalytic application for decolorization of methylene blue under UV irradiation. *Langmuir* **2004**, *20*, 7880−7883.
(46) Khan, M. M.; Lee, J.; Cho, M. H. Au@TiO2 nanocomposites for the catalytic degradation of methyl orange and methylene blue: An electron relay effect. *Ind. Eng. Chem. Res.* **2014**, *20*, 1584−1590.
(47) Kundu, S.; Mukadam, M. D.; Yusuf, S. M.; Jayachandran, M. Formation of shape-selective magnetic cobalt oxide nanowires: environmental application in catalysis studies. *CrystEngComm* **2013**, *15*, 482−497.
(48) Ganapuram, B. R.; Alle, M.; Dadigala, R.; Dasari, A.; Maragoni, V.; Guttena, V. Catalytic reduction of methylene blue and Congo red dyes using green synthesized gold nanoparticles capped by salmalia malabarica gum. *Int. Nano Lett.* **2015**, *5*, 215−222.
(49) Chen, M.; Liu, P.; Wang, C.; Ren, W.; Diao, G. Fast catalytic reduction of an azo dye by recoverable and reusable Fe_3O_4@PANI@Au magnetic composites. *New J. Chem.* **2014**, *38*, 4566−4573.
(50) Ujjain, S. K.; Sahu, V.; Sharma, R. K.; Singh, G. High performance, all solid state, flexible supercapacitor based on ionic liquid functionalized graphene. *Electrochim. Acta* **2015**, *157*, 245−251.

DOI: 10.1021/acsomega.8b00765
ACS Omega 2018, 3, 7846−7855

(51) Ahuja, P.; Sharma, R. K.; Singh, G. Solid-state, high-performance supercapacitor using graphene nanoribbons embedded with zinc manganite. *J. Mater. Chem. A* **2015**, *3*, 4931−4937.
(52) Ahuja, P.; Ujjain, S. K.; Kanojia, R. MnO_x/C nanocomposite: An insight on high-performance supercapacitor and non-enzymatic hydrogen peroxide detection. *Appl. Surf. Sci.* **2017**, *404*, 197−205.
(53) Ujjain, S. K.; Ahuja, P.; Sharma, R. K. Facile preparation of graphene nanoribbon/cobalt coordination polymer nanohybrid for non-enzymatic H_2O_2 sensing by dual transduction: electrochemical and fluorescence. *J. Mater. Chem. B* **2015**, *3*, 7614−7622.
(54) Ujjain, S. K.; Ahuja, P.; Sharma, R. K. Graphene nanoribbon wrapped cobalt manganite nanocubes for high performance all-solid-state flexible supercapacitors. *J. Mater. Chem. A* **2015**, *3*, 9925−9931.
(55) Wu, H.; Lin, S.; Chen, C.; Liang, W.; Liu, X.; Yang, H. A new ZnO/rGO/polyaniline ternary nanocomposite as photocatalyst with improved photocatalytic activity. *Mater. Res. Bull.* **2016**, *83*, 434−441.
(56) Zhang, L.; Jamal, R.; Zhao, Q.; Wang, M.; Abdiryim, T. Preparation of PEDOT/GO, PEDOT/MnO_2, and PEDOT/GO/MnO_2 nanocomposites and their application in catalytic degradation of methylene blue. *Nanoscale Res. Lett.* **2015**, *10*, 148.
(57) Kumar, R. Mixed phase lamellar titania-titanate anchored with Ag_2O and polypyrrole for enhanced adsorption and photocatalytic activity. *J. Colloid Interface Sci.* **2016**, *477*, 83−93.
(58) Benjwal, P.; Kumar, M.; Chamoli, P.; Kar, K. K. Enhanced photocatalytic degradation of methylene blue and adsorption of arsenic(III) by reduced graphene oxide (rGO)−metal oxide (TiO_2/Fe_3O_4) based nanocomposites. *RSC Adv.* **2015**, *5*, 73249−73260.
(59) Kumar, R.; El-Shishtawy, R.; Barakat, M. Synthesis and characterization of Ag-Ag_2O/TiO_2@polypyrrole heterojunction for enhanced photocatalytic degradation of methylene blue. *Catalysts* **2016**, *6*, 76.
(60) Kokane, S. B.; Sartale, S. D.; Betty, C. A.; Sasikala, R. Pd−TiO_2−$SrIn_2O_4$ heterojunction photocatalyst: enhanced photocatalytic activity for hydrogen generation and degradation of methylene blue. *RSC Adv.* **2014**, *4*, 55539−55547.

DOI: 10.1021/acsomega.8b00765
ACS Omega 2018, 3, 7846−7855